

Stability Analysis of Medial Axis Transform under Relative Hausdorff Distance

Sung Woo Choi and Seong-Whan Lee

Center for Artificial Vision Research, Korea University

Anam-dong, Seongbuk-ku, Seoul 136-701, Korea

Abstract

Medial axis transform (MAT) is a basic tool for shape analysis. But, in spite of its usefulness, it has some drawbacks, one of which is its instability under the boundary perturbation. To handle this problem in practical situations, various “pruning” methods have been proposed, which are usually heuristic in their nature and without sufficient error analyses. In this paper, we show that, although medial axis transform is unstable with respect to standard measures such as the Hausdorff distance, it is stable in a measure called relative Hausdorff distance for some “smoothed out” domains called injective domains. In fact, we obtain an upper bound of the relative Hausdorff distance of the MAT of an injective domain with respect to the MAT of an arbitrary domain which is in small Hausdorff distance from the original injective domain.

One consequence of the above result is that, by approximating a given domain with injective domains, we can extract the most “essential part” of the MAT within the prescribed error bound in Hausdorff distance. This introduces a new pruning strategy with precise error estimation. We also use the above result to introduce a new definition of MAT of bitmap images, which is both computable and conceptually natural. We illustrate our results with various examples.

Index Terms - medial axis transform, skeleton, stability analysis, relative Hausdorff distance, error bound, pruning

1 INTRODUCTION

Medial axis transform (**MAT** for short) is one of the basic tools widely used in shape analysis. Being natural conceptually, it extracts thinned features of a shape, which is homotopically equivalent to the original shape [1],[2],[3],[4]. It has a graph structure, which is simple to store and process in a computer. For these advantages, medial axis transform has a wide range of applications, such as biological shape recognition [5],[6],[7],[8],[9],[10],[11], character recognition and representation [12],[13],[14],[15],[16],[17], fingerprint classification [18], and visual analysis of circuit boards [19], to name a few.

MAT has a few equivalent definitions. One of them is the famous grassfire analogy [1], which defines the medial axis as the “quenching” points of the fire starting from the boundary. Another popular definition uses maximal inscribed circles, which we adopt in this paper; the *medial axis* (**MA**) of a plane domain is the set of the centers of the maximal inscribed circles contained in the given domain. The set of all the pairs of the medial axis point and the radius of the corresponding inscribed circle, is called the *medial axis transform*, which can be used to reconstruct the original domain. More explicitly, the medial axis transform **MAT**(Ω) and the medial axis **MA**(Ω) of a plane domain Ω is defined by

$$\mathbf{MAT}(\Omega) = \{ (p, r) \in \mathbb{R}^2 \times [0, \infty) \mid B_r(p) \text{ is a maximal ball contained in } \Omega \}$$

Stability Analysis of MAT

and

$$\mathbf{MA}(\Omega) = \{p \in \mathbb{R}^2 \mid \exists r \geq 0, \text{ such that } (p, r) \in \mathbf{MAT}(\Omega)\}.$$

One nuisance when dealing with medial axis (transform) is that it is not stable under the perturbation of the domain [20],[21]. This means that the transforms $\mathbf{MA} : \{\text{plane subsets}\} \rightarrow \{\text{plane subsets}\}$ and $\mathbf{MAT} : \{\text{plane subsets}\} \rightarrow \{\text{subsets in } \mathbb{R}^3\}$ are not continuous, where the domains and the images of the transforms are endowed with the Hausdorff distance. For example, the two domains (a) and (b) in Figure 1 are quite close in Hausdorff distance, but their medial axis (transform) differs drastically.

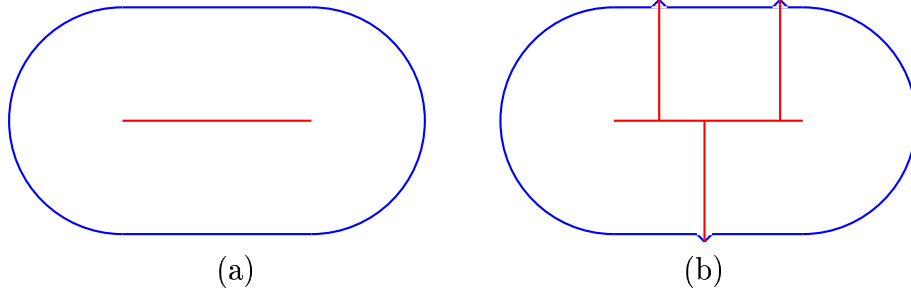


Figure 1: Instability of medial axis transform

In many practical situations, the domains in question are often given with small noises. This would produce undesirable results, since \mathbf{MA} (and \mathbf{MAT}) are not stable. A traditional alleviation of such phenomenon is the “pruning” methods which “cut off” the less important part of \mathbf{MA} (and \mathbf{MAT}) according to some measures [20],[22]. But in general, these methods are heuristic in determining what is the important part of \mathbf{MA} (and \mathbf{MAT}), and they often provide no underlying error estimations.

Stability Analysis of MAT

In this paper, we show that **MA** and **MAT** are indeed stable, if we concentrate on *relative Hausdorff distance* which will be defined later in this paper, instead of Hausdorff distance. We will prove that, when a plane domain Ω satisfies a certain smoothness condition called the *injectivity*, then the *relative Hausdorff distance* of **MA**(Ω) (*resp.*, **MAT**(Ω)) with respect to **MA**(Ω') (*resp.*, **MAT**(Ω')) goes to zero, if the Hausdorff distances between $\partial\Omega$, $\partial\Omega'$ and between Ω , Ω' go to zero for arbitrary domain Ω' . This is achieved by first deriving an upper bound formula for **MA** and **MAT** errors, which depends on the given injective domain.

We show how this result can be utilized in a new pruning strategy; by approximating a given domain with injective domains, we can guarantee that the **MA** (and the **MAT**) of the approximating domain are the most “essential parts” of the **MA** (and the **MAT**) of the original domain within a prescribed error bound in Hausdorff distance. For example, the domain in Figure 2 (a) is approximated by an injective domain in Figure 2 (b), which means that the Hausdorff distance between the two domains is small. Although the Hausdorff distance between the **MA**s (and the **MAT**s) of the two domains is large, the relative Hausdorff distance of the approximating **MA** (and **MAT**) in Figure 2 (b) with respect to the original **MA** (and **MAT**) in Figure 2 (a) is small. Furthermore, if we approximate the domain in Figure 2 (a) with another injective domain, we can bound the Hausdorff distance between the two approximating **MA**s (and **MAT**s). This, in effect, prunes the hairy **MA** (and **MAT**) in Figure 2 (a), and extracts the most essential part of it.

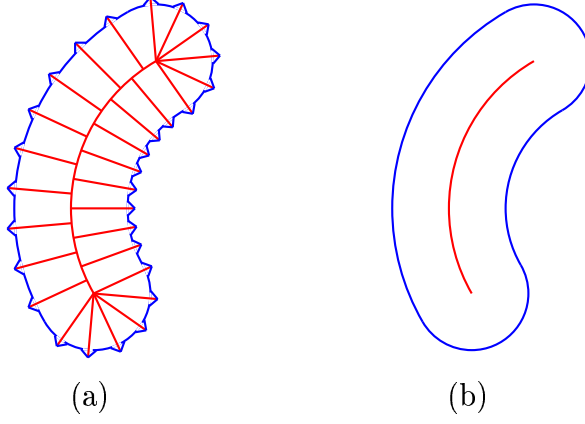


Figure 2: Essential part of medial axis (transform)

In principle, this amounts to a pruning by boundary smoothing. But we stress here that, unlike the previous known methods such as Curvature Flow Smoothing [23],[24],[25],[26],[27],[28], our method is equipped with precise error analysis.

We also use the stability of **MA** (and **MAT**) under relative Hausdorff distance to introduce a new definition of **MA** (and **MAT**) of the bitmap images. For the bitmap images, various definitions of **MA** (and **MAT**) have been proposed [2],[3] with a view to the thinning methods. But, being devised mostly for computational purposes, they lack the theoretical naturalness in general. Our definition has conceptual naturalness as well as computational amenability.

In Section 2, we briefly review the basic mathematical results on medial axis transform, which is needed to understand the further analysis. We also introduce the relative Hausdorff distance, and list some fundamental properties. The main stability results are proved in Section 3, and a few simple examples are given in Section 4 for the illustration of the main result. In Section 5, we show how the

result in Section 3 can be used in pruning by applying it to a more realistic and complex example. Here, we also give a new definition of **MA** and **MAT** of the bitmap images. Finally, we summarize our results in Section 6.

2 PRELIMINARIES

2.1 NORMAL DOMAINS AND THEIR MAT

To facilitate the later analysis, some preliminary understanding of medial axis transform is needed. In this section, we briefly review some mathematical facts about medial axis transform of plane domains, and present a few terminologies used in this paper.

For completeness, we first restrict the kind of the domains we deal with to what we call the *normal domains*. Although it is often neglected in literature, this restriction is necessary for reasonable behaviours of **MA** and **MAT**. We will call a subset Ω of \mathbb{R}^2 a *normal domain*, if it satisfies the following two conditions:

- Ω is compact, or equivalently, Ω is closed and bounded.
- The boundary $\partial\Omega$ of Ω is a (disjoint) union of finite number of simple closed curves, each of which in turn consists of finite number of real analytic curve pieces.

With normal domains, the following expected behaviour of **MA** and **MAT** turns out to be true.

Proposition 1 ([4]) *Let Ω be a normal domain in \mathbb{R}^2 . Then both **MA**(Ω) and **MAT**(Ω) have finite graph structures.*

Stability Analysis of MAT

Here, by the finite graph structure, we mean that \mathbf{MA} and \mathbf{MAT} consist of finitely many curve pieces, and they meet each other at only finitely many points.

There are examples with which the above result can be violated. In fact, there exist domains with their medial axes having infinitely many “leaves” and thus violating Proposition 1, which satisfy all the above normality conditions except the real-analyticity is replaced by the C^∞ condition [4]. In the extreme case when Ω has a fractal structure, $\mathbf{MA}(\Omega)$ can even have the fractal dimension greater than 1 [29]. But in practical situations, almost all domains considered are normal. So it is natural to focus on the normal domains, for which the medial axis transform behaves reasonably as is usually expected. For these reasons, we will only consider the normal domains in this paper.

Let Ω be a normal domain, and let $(p, r) \in \mathbf{MAT}(\Omega)$. So $B_r(p)$ is a maximal ball in Ω . We will call $\partial B_r(p)$, the boundary of $B_r(p)$, a *contact circle* of Ω . The number of the connected components in $B_r(p) \cap \partial\Omega$ is equal to the number of the ‘prongs’ of $\mathbf{MA}(\Omega)$ emanating from p . Each point in $B_r(p) \cap \partial\Omega$ is called a *contact point*, and a connected component of $B_r(p) \cap \partial\Omega$ which constitutes a circular arc is called a *contact arc*. See Figure 3. We call p an *n-prong point* ($n \geq 1$), when n is the number of the prongs of $\mathbf{MA}(\Omega)$ emanating from p . For example, the point p in Figure 3 is a 3-prong point. It has been proved [4] that, except for finitely many points, $\mathbf{MA}(\Omega)$ consists of only the 2-prong points, and a point in $\mathbf{MA}(\Omega)$ is a 1-prong point, if and only if it is an end point of $\mathbf{MA}(\Omega)$. Later in Section 3, we will classify the 1-prong points in more detail.

Stability Analysis of MAT

A corner point in $\partial\Omega$ is called a *sharp corner* (*resp.*, *dull corner*), if the angle of the corner inside the domain is less than (*resp.*, greater than) π . A sharp corner always introduces an end point of $\mathbf{MA}(\Omega)$, *i.e.*, a 1-prong point.

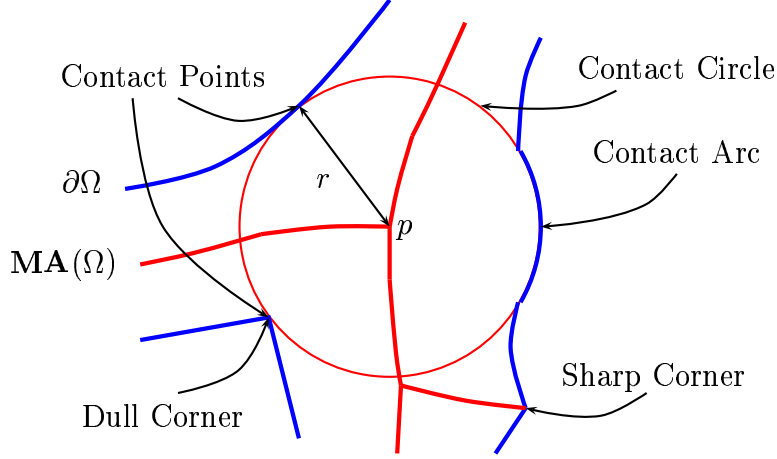


Figure 3: Contact circle and n -prong point

Let Ω be a normal domain, and let $(p, r) \in \mathbf{MAT}(\Omega)$. We will introduce a few domain-dependent constants. First, define ρ_Ω by

$$\rho_\Omega = \inf_{(p,r) \in \mathbf{MAT}(\Omega)} r,$$

i.e., the smallest radius of the contact circles of Ω . Note that $\rho_\Omega = 0$, if and only if Ω has a sharp corner.

Suppose p is a 2-prong point. Suppose also that $B_r(p)$ has no contact arcs. In fact, almost all points in $\mathbf{MA}(\Omega)$ except finitely many ones are of this kind. We will denote by $G(\Omega)$, the subset of $\mathbf{MA}(\Omega)$ consisting of all the 2-prong points with no contact arcs. Let p_1 and p_2 be the two contact points corresponding to p . (See Figure 4.) Define $0 < \theta(p) \leq \pi/2$ by the angle between $\overline{pp_1}$ (or equivalently,

Stability Analysis of MAT

$\overline{pp_2})$ and the tangent direction of $\mathbf{MA}(\Omega)$ at p . Define θ_Ω by

$$\theta_\Omega = \inf \{ \theta(p) : p \in G(\Omega) \}.$$

Note that $\theta_\Omega > 0$, if and only if every 1-prong point of $\mathbf{MA}(\Omega)$ is of the type (c) in Figure 7.

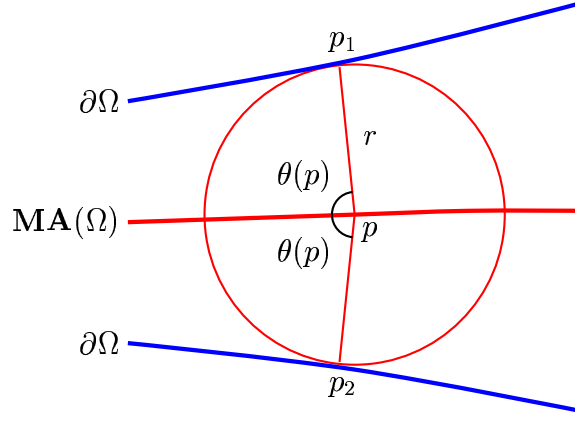


Figure 4: 2-Prong point in $G(\Omega)$

2.2 RELATIVE HAUSDORFF DISTANCE

Hausdorff distance is one of the most popular and intuitively appealing measures of the difference between two sets [30],[31]. We present briefly here the definitions and its elementary properties. We also introduce the concept *relative Hausdorff distance*, with which we later prove the stability of **MA** and **MAT**.

Let A and B be two (closed) subsets in \mathbb{R}^n for some $n \geq 1$. The *relative Hausdorff distance* of A with respect to B , $\mathcal{H}(A|B)$, is defined by

$$\mathcal{H}(A|B) = \max_{p \in A} d(p, B),$$

Stability Analysis of MAT

where $d(\cdot, \cdot)$ is the usual Euclidean distance in \mathbb{R}^n . Intuitively speaking, it is the smallest real number ϵ for which A is contained in the ϵ -neighborhood of B . The relative Hausdorff distance $\mathcal{H}(A|B)$ of A with respect to B is less than ϵ , if and only if A is contained in the ϵ -neighborhood of B . Thus, relative Hausdorff distance measures how a set is contained in another set. See Figure 5.

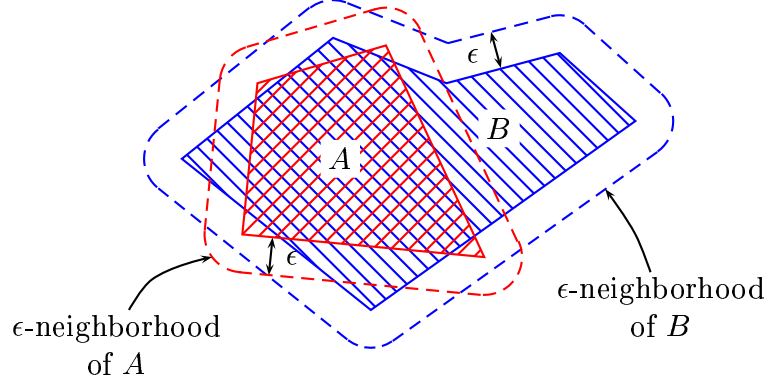


Figure 5: Relative Hausdorff distance : $\mathcal{H}(A|B) < \epsilon$ but $\mathcal{H}(A, B) \not< \epsilon$

The *Hausdorff distance* between A and B , $\mathcal{H}(A, B)$, is defined by

$$\begin{aligned} \mathcal{H}(A, B) &= \max \left\{ \max_{p \in A} d(p, B), \max_{q \in B} d(q, A) \right\} \\ &= \max \{ \mathcal{H}(A|B), \mathcal{H}(B|A) \}, \end{aligned}$$

i.e., it is the maximum of the relative Hausdorff distance of A with respect to B and the relative Hausdorff distance of B with respect to A . The Hausdorff distance between two sets A and B is less than $\epsilon > 0$, if and only if A is contained in the ϵ -neighborhood of B , and B is contained in the ϵ -neighborhood of A . Thus, Hausdorff distance measures how much close the shapes of two sets are. See Figure 6. Note that, in Figure 5, the Hausdorff distance $\mathcal{H}(A, B)$ is large

Stability Analysis of MAT

$(\mathcal{H}(A, B) \not\leq \epsilon)$, whereas the relative Hausdorff $\mathcal{H}(A|B)$ is small ($\mathcal{H}(A|B) < \epsilon$).

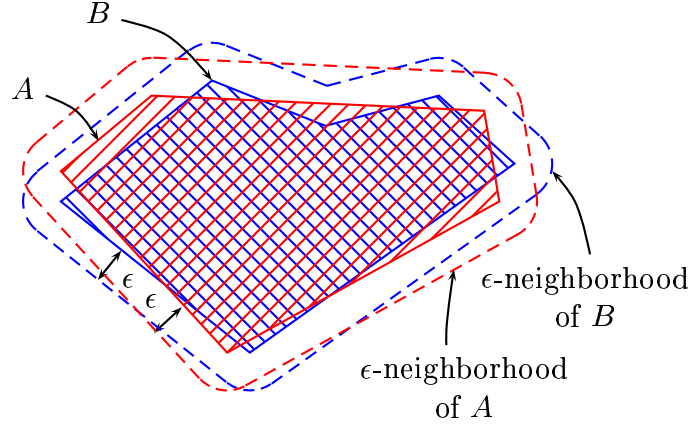


Figure 6: Hausdorff Distance : $\mathcal{H}(A, B) < \epsilon$

The followings are basic properties of Hausdorff distance for any closed sets A , B and C in \mathbb{R}^n ($n \geq 1$):

$$\mathcal{H}(A, B) \geq 0. \tag{1}$$

$$\mathcal{H}(A, B) = \mathcal{H}(B, A). \tag{2}$$

$$\mathcal{H}(A, C) \leq \mathcal{H}(A, B) + \mathcal{H}(B, C). \tag{3}$$

Here, the equality in (1) holds, if and only if $A = B$, and (3) is called the *triangle inequality* for Hausdorff distance.

3 STABILITY OF MAT

In this section, we show that **MA** and **MAT** are stable under relative Hausdorff distance, for some special kind of plane domains which we will call *injective*. In a sense, injective domains are some kinds of “smoothed out” or “rounded off” ones of ordinary normal domains.

Definition 1 (Injective Domain)

A normal domain Ω in \mathbb{R}^2 is called injective, if $\rho_\Omega > 0$ and $\theta_\Omega > 0$.

Let Ω be a normal domain. It is easy to see that there are exactly three kinds of 1-prong points in $\mathbf{MA}(\Omega)$. See Figure 7: Type (a) is the center of a maximal circle with only one contact point at which the circle osculates the boundary. Type (b) is a sharp corner. Type (c) is a 1-prong point with a contact arc.

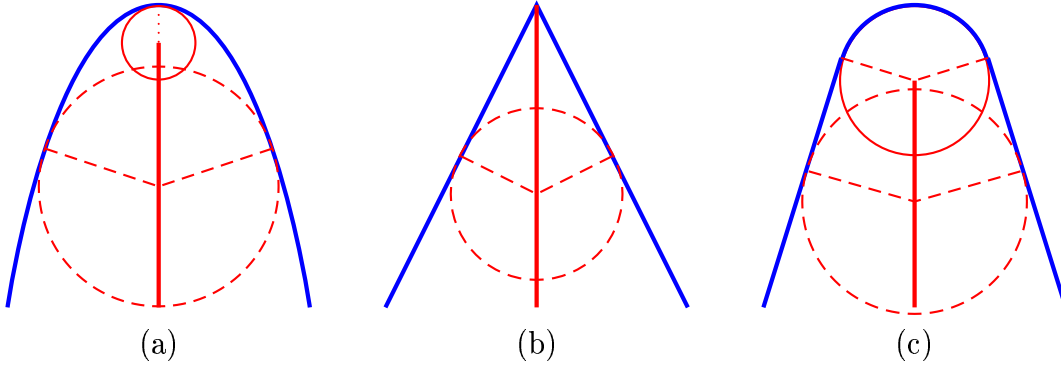


Figure 7: Three types of 1-prong points

Suppose Ω is an injective domain. Then every 1-prong point of $\mathbf{MA}(\Omega)$ cannot be of Type (a) or Type (b) in Figure 7: If $\mathbf{MA}(\Omega)$ has a 1-prong point of Type (a) or Type (b), then we would have either $\theta_\Omega = 0$ or $\rho_\Omega = 0$. Conversely, it is obvious that Ω is injective if every 1-prong point of $\mathbf{MA}(\Omega)$ is of Type (c) in Figure 7. Thus Ω is injective, if and only if every 1-prong point of $\mathbf{MA}(\Omega)$ is of Type (c) in Figure 7.

Note that, if we cut out a small segment of \mathbf{MA} near every 1-prong point of Type (a) and (b), then the resulting domain is an injective domain. So, an

Stability Analysis of MAT

injective domain can be obtained by smoothing an arbitrary normal domain.

Now we start our stability analysis. Let Ω be a normal domain. First, note that, for every p in the interior of Ω , $\text{int}\Omega$, there exists a unique $(\phi(p), r) \in \mathbf{MAT}(\Omega)$ such that $\overline{pp_1} \subset \overline{\phi(p)p_1}$ for some $p_1 \in \partial B_r(\phi(p)) \cap \partial\Omega$. See Figure 8.

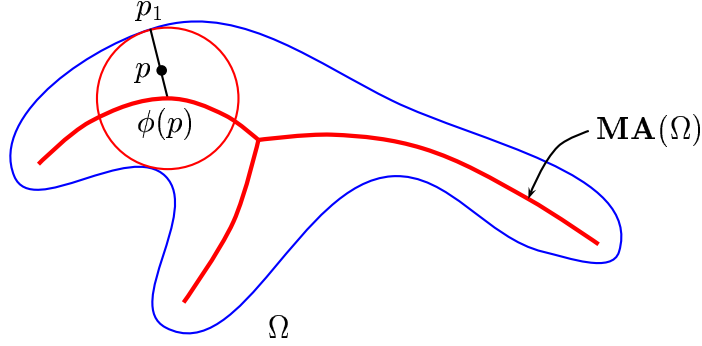


Figure 8: Correspondence between p and $\phi(p)$

Lemma 1 *Let Ω be a normal domain, and let $p \in \text{int}\Omega$. Let $\phi(p)$ and p_1 be the (unique) points in $\mathbf{MA}(\Omega)$ and in $\partial\Omega$ respectively, corresponding to p in the above sense. Let $\eta = |p - \phi(p)|$, and let q be the (unique) point in $\partial B_{r+\eta}(\phi(p)) \cap l(\theta)$, where $l(\theta)$ is the half-line starting from p in the direction which has the angle θ ($0 \leq \theta \leq \pi$) from the vector $\overrightarrow{\phi(p)p_1}$. Figure 9 illustrates the situation. Let $D(\theta)$ be the distance between p and q . Then we have*

$$D(\theta) = -\eta \cos \theta + \sqrt{\eta^2 \cos^2 \theta + (r + \eta)^2 - \eta^2},$$

where $r = d(p, p_1) = d(p, \partial\Omega)$.

Proof. First, note that $\overline{pp_1} \subset \overline{\phi(p)p_1}$. Let $0 \leq \phi \leq \pi$ be the angle between $\overrightarrow{\phi(p)p}$ and $\overrightarrow{\phi(p)p_1}$.

Stability Analysis of MAT

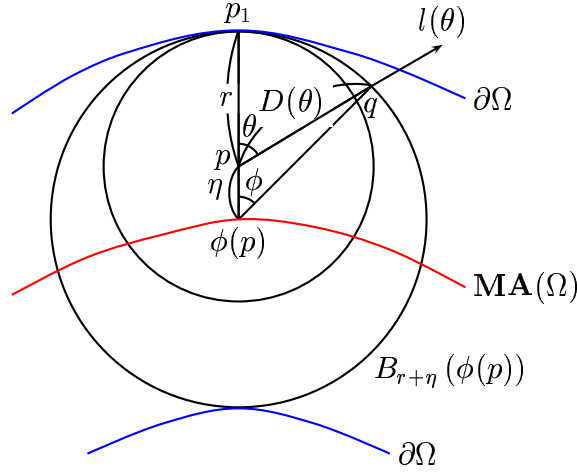


Figure 9: Illustration for the proof of Lemma 1

Note that

$$(r + \eta) \cos \phi - D(\theta) \cos \theta = \eta,$$

from which it follows that

$$\cos \phi = \frac{\eta + D(\theta) \cos \theta}{r + \eta}. \quad (4)$$

Now, from the cosine formula for the triangle $\triangle pq\phi(p)$, we have

$$D(\theta)^2 = (r + \eta)^2 + \eta^2 - 2\eta(r + \eta) \cos \phi, \quad (5)$$

and so, by substituting (4) into (5), we get

$$D(\theta)^2 = (r + \eta)^2 - \eta^2 - 2\eta D(\theta) \cos \theta,$$

or

$$D(\theta)^2 + 2\eta \cos \theta \cdot D(\theta) - \{(r + \eta)^2 - \eta^2\} = 0. \quad (6)$$

Solving the equation (6) yields the solution

$$D(\theta) = -\eta \cos \theta + \sqrt{\eta^2 \cos^2 \theta + (r + \eta)^2 - \eta^2},$$

Stability Analysis of MAT

since we know that $D(\theta) > 0$. This completes the proof. \square

Now we introduce a function corresponding to each injective domain, which will play an important role for the upper bounds of **MA** and **MAT** errors.

Definition 2 *Let Ω be an injective domain. Then we define $\eta_\Omega : [0, \infty) \rightarrow [0, \infty)$ by*

$$\eta_\Omega(x) = \frac{\rho_\Omega \cdot x}{\rho_\Omega \sin^2(\theta_\Omega/2) - x \cos^2(\theta_\Omega/2)}.$$

We present without proof a straightforward but noteworthy property of the function η_Ω .

Lemma 2 *Let Ω be an injective domain. Then, $\eta_\Omega(x) > 0$ when $0 < x < \rho_\Omega \tan^2 \theta_\Omega/2$, and $\lim_{x \rightarrow 0} \eta_\Omega(x) = 0$.*

Now we present the main theorem of this section. See Appendix for a proof.

Theorem 1 *Let Ω be an injective domain, and let Ω' be a normal domain with $\mathcal{H}(\partial\Omega, \partial\Omega') < \epsilon$ and $\mathcal{H}(\Omega, \Omega') < \epsilon$, where $\epsilon < \min\{\rho_\Omega \tan^2 \theta_\Omega/2, \rho_\Omega/2\}$. Then we have*

$$\mathcal{H}(\mathbf{MA}(\Omega) | \mathbf{MA}(\Omega')) < \eta_\Omega(\epsilon),$$

and

$$\mathcal{H}(\mathbf{MAT}(\Omega) | \mathbf{MAT}(\Omega')) < \sqrt{\eta_\Omega(\epsilon)^2 + \{\epsilon + \eta_\Omega(\epsilon)\}^2}.$$

The above theorem, together with Lemma 2, tells us that **MA** and **MAT** of injective domains are indeed stable under relative Hausdorff distance. Thus, when we deform an injective domain continuously (with respect to Hausdorff distance),

Stability Analysis of MAT

the **MA** and the **MAT** of the original injective domain deviates continuously (with respect to relative Hausdorff distance) from the **MA**s and the **MAT**s of the deformed domains. More explicitly, we have:

Corollary 1 *Let Ω be an injective domain. Then, for every $\eta > 0$, there exists $\epsilon > 0$ such that*

$$\mathcal{H}(\mathbf{MA}(\Omega) | \mathbf{MA}(\Omega')) < \eta$$

and

$$\mathcal{H}(\mathbf{MAT}(\Omega) | \mathbf{MAT}(\Omega')) < \eta$$

for any normal domain Ω' with $\mathcal{H}(\partial\Omega, \partial\Omega') < \epsilon$ and $\mathcal{H}(\Omega, \Omega') < \epsilon$.

Proof. This follows easily from Theorem 1 and Lemma 2. □

Theorem 1 and Corollary 1 also say that **MA** (*resp.*, **MAT**) of an injective domain is approximately a *maximal common* part of the **MA** (*resp.*, the **MAT**) of any domain sufficiently close to the original injective domain in Hausdorff distance.

4 ILLUSTRATING EXAMPLES

In this section, we show a few examples of injective domains to illustrate the result in Section 3. With each example, we will calculate the error bound explicitly.

4.1 STADIUM (NOT TAPERED)

Let Ω be a stadium (not tapered) depicted in Figure 10.

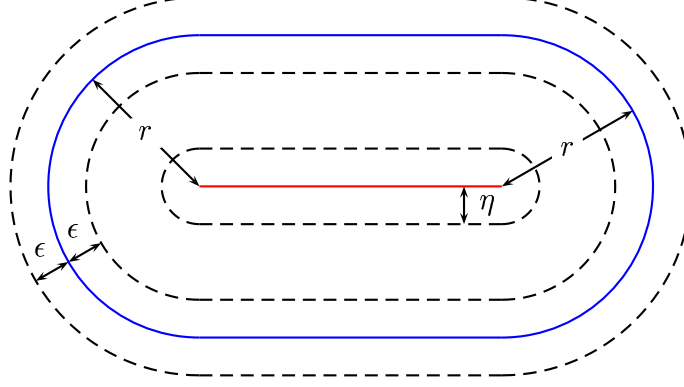


Figure 10: Error analysis for non-tapered stadium

It is clear that $\rho_\Omega = r$ and $\theta_\Omega = \pi/2$. So we have

$$\eta_\Omega(\epsilon) = \frac{\epsilon r}{r \cdot \frac{1}{2} - \epsilon \cdot \frac{1}{2}} = \frac{2\epsilon r}{r - \epsilon} = \frac{2\epsilon}{1 - (\epsilon/r)}.$$

Now, by Theorem 1, we have

$$\mathcal{H}(\mathbf{MA}(\Omega)|\mathbf{MA}(\Omega')) < \frac{2\epsilon}{1 - (\epsilon/r)},$$

and

$$\begin{aligned} \mathcal{H}(\mathbf{MAT}(\Omega)|\mathbf{MAT}(\Omega')) &< \sqrt{\left\{\frac{2\epsilon}{1 - (\epsilon/r)}\right\}^2 + \left\{\frac{2\epsilon}{1 - (\epsilon/r)} + \epsilon\right\}^2} \\ &= \frac{\epsilon\sqrt{4 + \{3 - (\epsilon/r)\}^2}}{1 - (\epsilon/r)}, \end{aligned}$$

for every $0 < \epsilon < \min\{r \tan^2(\pi/4), r/2\} = r/2$ and for every normal domain Ω'

such that $\mathcal{H}(\partial\Omega, \partial\Omega') < \epsilon$ and $\mathcal{H}(\Omega, \Omega') < \epsilon$.

4.2 RIBBON

Let Ω be a ribbon with constant width (See Figure 11). Then, since we have

$\rho_\Omega = r$ and $\theta_\Omega = \pi/2$, the result is the same with the non-tapered stadium

analyzed in Section 4.1.

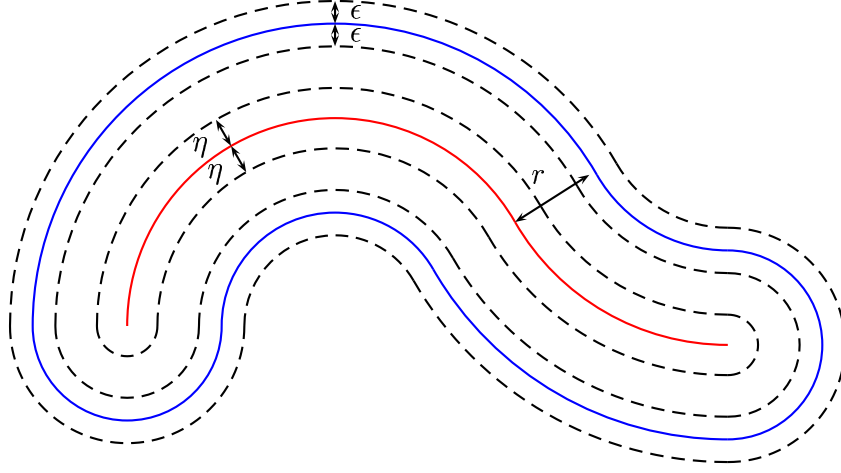


Figure 11: Error analysis for ribbon

4.3 ROUNDED RECTANGLE

Let Ω be a rectangle with each corner rounded off by a circular ball of radius r .

See Figure 12. Clearly, we have $\rho_\Omega = r$ and $\theta_\Omega = \pi/4$.

So

$$\eta_\Omega(\epsilon) = \frac{\epsilon r}{r \cdot \frac{\sqrt{2}-1}{2\sqrt{2}} - \epsilon \cdot \frac{\sqrt{2}+1}{2\sqrt{2}}} = \frac{2\sqrt{2} \cdot \epsilon}{(\sqrt{2}-1) - (\sqrt{2}+1)(\epsilon/r)}.$$

Thus, for any $0 < \epsilon < \min\{r \tan^2 \pi/8, r/2\} = (3 - 2\sqrt{2})r$, we have

$$\mathcal{H}(\mathbf{MA}(\Omega)|\mathbf{MA}(\Omega')) < \frac{2\sqrt{2} \cdot \epsilon}{(\sqrt{2}-1) - (\sqrt{2}+1)(\epsilon/r)}$$

and

$$\begin{aligned} \mathcal{H}(\mathbf{MAT}(\Omega)|\mathbf{MAT}(\Omega')) &< \sqrt{\eta_\Omega(\epsilon)^2 + \{\epsilon + \eta_\Omega(\epsilon)\}^2} \\ &= \frac{\epsilon \sqrt{8 + \{(3\sqrt{2}-1) - (\sqrt{2}+1)(\epsilon/r)\}^2}}{(\sqrt{2}-1) - (\sqrt{2}+1)(\epsilon/r)}, \end{aligned}$$

for any normal domain Ω' such that $\mathcal{H}(\partial\Omega, \partial\Omega') < \epsilon$ and $\mathcal{H}(\Omega, \Omega') < \epsilon$.

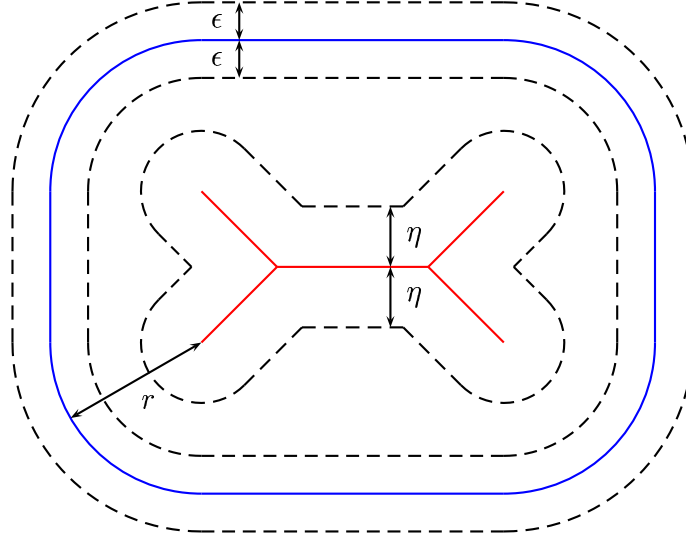


Figure 12: Error analysis for rounded rectangle

4.4 TAPERED STADIUM

Let Ω be a stadium tapered by an angle θ . See Figure 13. Here we have $\rho_\Omega = r$ and $\theta_\Omega = \theta$.

So we have

$$\eta_\Omega(\epsilon) = \frac{\epsilon r}{r \sin^2 \theta/2 - \epsilon \cos^2 \theta/2} = \frac{\epsilon}{\sin^2 \theta/2 - \cos^2 \theta/2 \cdot (\epsilon/r)}.$$

Thus, for any $0 < \epsilon < \min \{r \tan^2 \theta/2, r/2\}$, we have

$$\mathcal{H}(\mathbf{MA}(\Omega)|\mathbf{MA}(\Omega')) < \frac{\epsilon}{\sin^2 \theta/2 - \cos^2 \theta/2 \cdot (\epsilon/r)}$$

and

$$\begin{aligned} \mathcal{H}(\mathbf{MA}(\Omega)|\mathbf{MA}(\Omega')) &< \sqrt{\eta_\Omega(\epsilon)^2 + \{\epsilon + \eta_\Omega(\epsilon)\}^2} \\ &= \frac{\epsilon \sqrt{1 + \{1 + \sin^2 \theta/2 - \cos^2 \theta/2 \cdot (\epsilon/r)\}^2}}{\sin^2 \theta/2 - \cos^2 \theta/2 \cdot (\epsilon/r)}, \end{aligned}$$

for every normal domain Ω' such that $\mathcal{H}(\partial\Omega, \partial\Omega') < \epsilon$ and $\mathcal{H}(\Omega, \Omega') < \epsilon$.

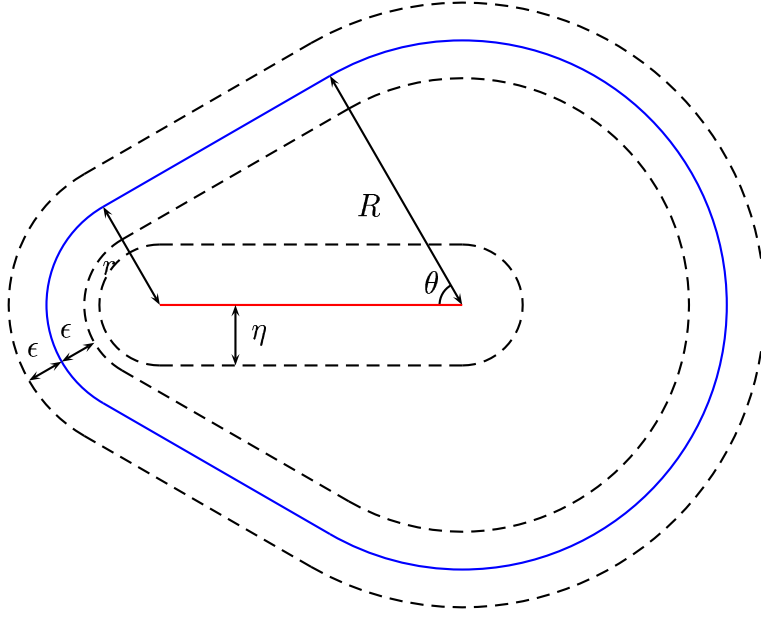


Figure 13: Error analysis for tapered stadium

5 APPLICATION TO PRUNING : EXTRACTING THE MOST ESSENTIAL PART

We have seen that **MA** and **MAT** of injective domains are stable under relative Hausdorff distance. But still, it is true that they are unstable under Hausdorff distance. However, their stability under relative Hausdorff distance can be utilized to extract the “most essential” part of a normal domain approximately.

Suppose we perturb an injective domain with domains which are also injective. In this case, **MA** and **MAT** become stable under “Hausdorff distance”, not only under relative Hausdorff distance.

Theorem 2 *Let Ω_1 and Ω_2 be two injective domains, and let $\rho = \min \{\rho_{\Omega_1}, \rho_{\Omega_2}\}$, $\theta = \min \{\theta_{\Omega_1}, \theta_{\Omega_2}\}$. Suppose $\mathcal{H}(\partial\Omega_1, \partial\Omega_2) < \epsilon$ and $\mathcal{H}(\Omega_1, \Omega_2) < \epsilon$, where $0 < \epsilon <$*

Stability Analysis of MAT

$\min \{\rho \tan^2 \theta/2, \rho/2\}$. Then we have

$$\mathcal{H}(\mathbf{MA}(\Omega_1), \mathbf{MA}(\Omega_2)) < \eta$$

and

$$\mathcal{H}(\mathbf{MAT}(\Omega_1), \mathbf{MAT}(\Omega_2)) < \sqrt{\eta^2 + (\epsilon + \eta)^2},$$

where

$$\eta = \frac{\rho\epsilon}{\rho \sin^2 \theta/2 - \epsilon \cos^2 \theta/2}.$$

Proof. By Theorem 1, we have $\mathcal{H}(\mathbf{MA}(\Omega_1)|\mathbf{MA}(\Omega_2)) < \eta$ and $\mathcal{H}(\mathbf{MAT}(\Omega_1)|\mathbf{MAT}(\Omega_2)) < \sqrt{\eta^2 + (\epsilon + \eta)^2}$. With a symmetric argument, we also have $\mathcal{H}(\mathbf{MA}(\Omega_2)|\mathbf{MA}(\Omega_1)) < \eta$ and $\mathcal{H}(\mathbf{MAT}(\Omega_2)|\mathbf{MAT}(\Omega_1)) < \sqrt{\eta^2 + (\epsilon + \eta)^2}$. Thus we have $\mathcal{H}(\mathbf{MA}(\Omega_1), \mathbf{MA}(\Omega_2)) < \eta$ and $\mathcal{H}(\mathbf{MAT}(\Omega_1), \mathbf{MAT}(\Omega_2)) < \sqrt{\eta^2 + (\epsilon + \eta)^2}$ by the definition of Hausdorff distance. \square

Now suppose we approximate a normal domain with two different injective domains. Theorem 1 tells us that the **MA** and the **MAT** of each injective domain are “approximately” contained in the **MA** and the **MAT** of the approximated domain respectively. Meanwhile, since the two injective domains themselves are in small Hausdorff distance by the triangle inequality for Hausdorff distance (See Equation (3) in Section 2), we can also see from Theorem 2 that the **MA** and the **MAT** of the approximating injective domains are close in Hausdorff distance respectively. More specifically, we have the following:

Theorem 3 *Let Ω be a normal domain, and let Ω_1 and Ω_2 be two injective domains. Let $\rho = \min \{\rho_{\Omega_1}, \rho_{\Omega_2}\}$ and $\theta = \min \{\theta_{\Omega_1}, \theta_{\Omega_2}\}$. Suppose $\mathcal{H}(\partial\Omega_i, \partial\Omega) <$*

Stability Analysis of MAT

ϵ and $\mathcal{H}(\Omega_i, \Omega) < \epsilon$ for $i = 1, 2$, where $0 < 2\epsilon < \min \{\rho \tan^2 \theta/2, \rho/2\}$. Then we have

$$\mathcal{H}(\mathbf{MA}(\Omega_1), \mathbf{MA}(\Omega_2)) < \eta$$

and

$$\mathcal{H}(\mathbf{MAT}(\Omega_1), \mathbf{MAT}(\Omega_2)) < \sqrt{\eta^2 + (2\epsilon + \eta)^2},$$

where

$$\eta = \frac{2\rho\epsilon}{\rho \sin^2 \theta/2 - 2\epsilon \cos^2 \theta/2}.$$

Proof. The proof follows immediately from Theorem 2 and the triangle inequality (3) in Section 2. \square

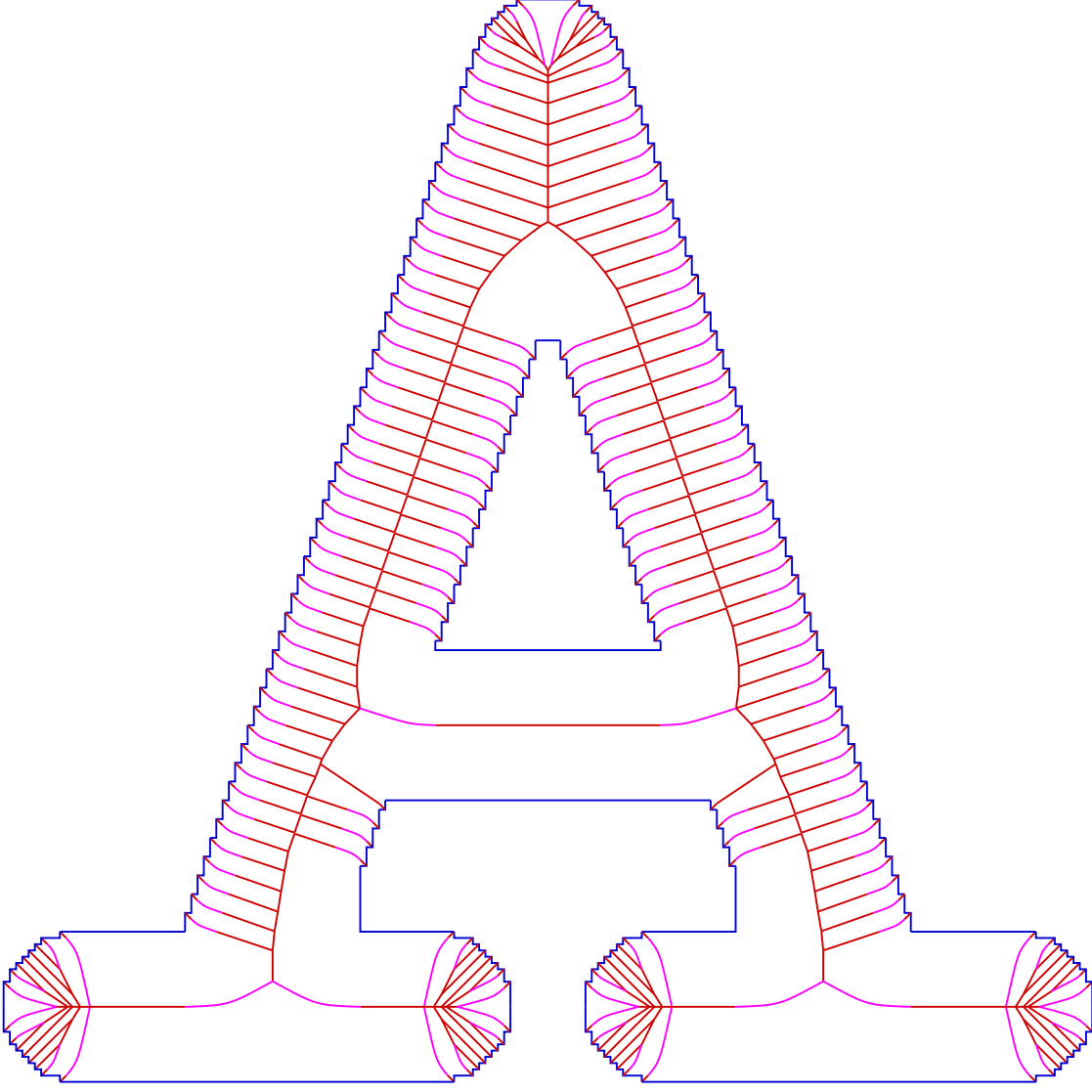
In short, with respect to Hausdorff distance, **MA** and **MAT** change continuously, when we change the approximating injective domain continuously. Thus the choice of the injective domain to approximate a normal domain does not affect the resulting **MA** and **MAT** much. We have noticed from Theorem 1 that **MA** and **MAT** of an injective domain are approximately a maximal common part of those of every approximated domain. Now an important point of Theorem 3 is that it sets an error bound of **MA** and **MAT** in Hausdorff distance, which may arise from the choice of the approximating injective domain.

From these considerations, we can propose a new pruning strategy which approximates the original domain with appropriate injective domains. This makes it possible to extract the maximal common, or the most essential part of **MA** and **MAT** within an error bound that depend on the constants such as ρ , θ , ϵ . Of course, as we vary these constants (that is, as we vary the approximating injective

domains), we can obtain the essential part of **MA** and **MAT** with varying degrees of fine details.

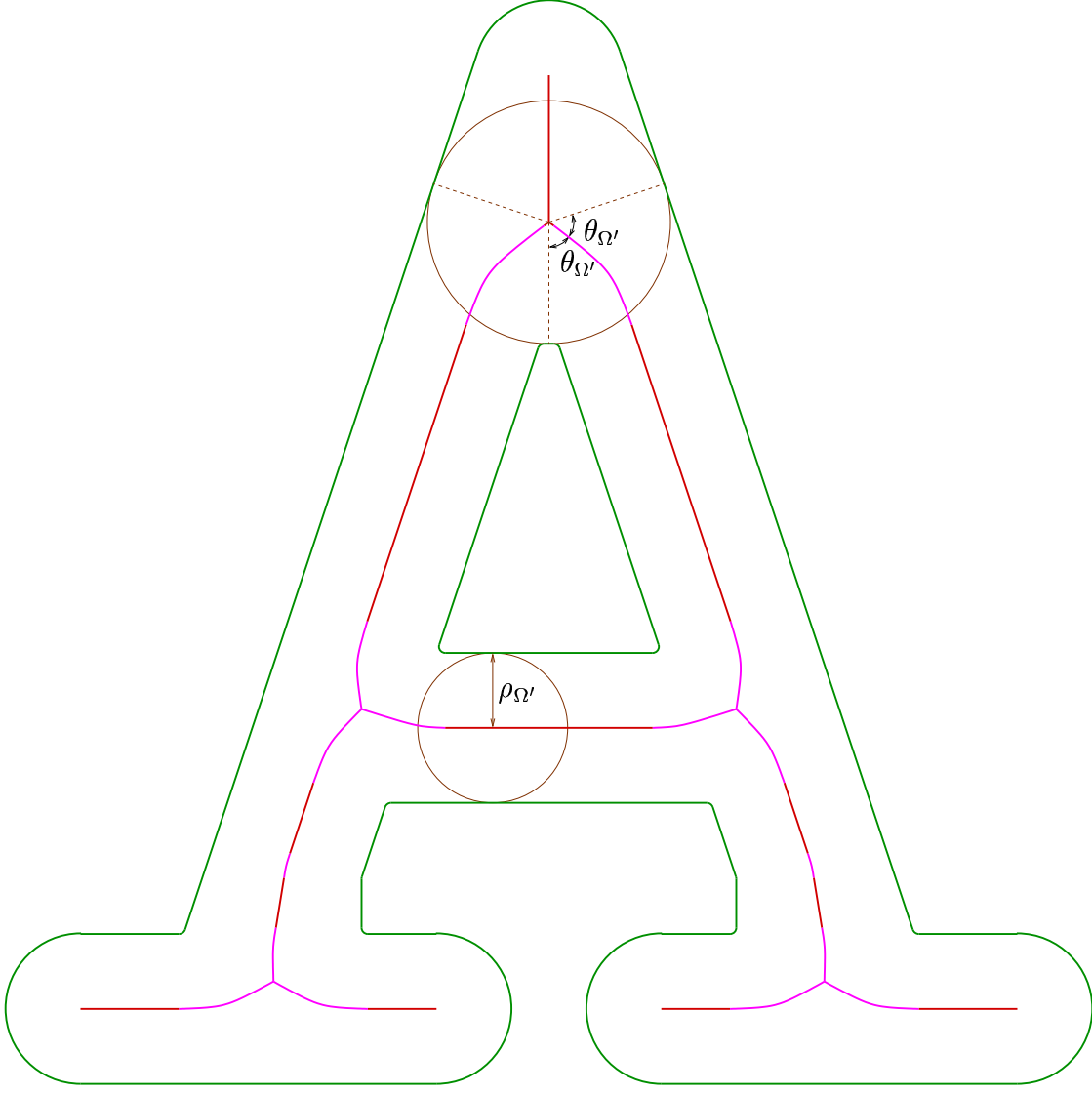
For example, let Ω be the domain depicted in Figure 14. The **MA** shown has many hairy parts due to the zigzag nature of the boundary, which is a common characteristic of the bitmap figures. We approximated Ω with an injective domain Ω' with $\rho_{\Omega'} = 1200$ and $\theta_{\Omega'} = 54.19425477^\circ$ shown in Figure 15. The Hausdorff distances $\mathcal{H}(\partial\Omega, \partial\Omega')$ and $\mathcal{H}(\Omega, \Omega')$ are less than $\epsilon = 37.5$. In Figure 16, Ω and Ω' are shown overlapping each other. Now by Theorem 1, it follows that $\mathcal{H}(\mathbf{MA}(\Omega')|\mathbf{MA}(\Omega)) < 205.2384901$ and $\mathcal{H}(\mathbf{MAT}(\Omega')|\mathbf{MAT}(\Omega)) < 317.8754668$. See Figure 17 to note how approximately $\mathbf{MA}(\Omega')$ is contained in $\mathbf{MA}(\Omega)$. Furthermore, if we approximate Ω with another injective domain Ω'' with $\rho_{\Omega''} \geq \rho_{\Omega'}$, $\theta_{\Omega''} \geq \theta_{\Omega'}$, $\mathcal{H}(\partial\Omega, \partial\Omega'') < \epsilon$ and $\mathcal{H}(\Omega, \Omega'') < \epsilon$, then Theorem 3 guarantees that $\mathcal{H}(\mathbf{MA}(\Omega'), \mathbf{MA}(\Omega'')) < 474.8397268$ and $\mathcal{H}(\mathbf{MAT}(\Omega'), \mathbf{MAT}(\Omega'')) < 726.4960366$. Thus we can say that $\mathbf{MA}(\Omega')$ (*resp.*, $\mathbf{MAT}(\Omega')$) is the most essential part of $\mathbf{MA}(\Omega)$ (*resp.*, $\mathbf{MAT}(\Omega)$) within the upper bound of Hausdorff distance 474.8397268 (*resp.*, 726.4960366) with the fine details specified by the constants ϵ , $\rho_{\Omega'}$ and $\theta_{\Omega'}$.

We can also use Theorem 3 to make a new definition of **MA** and **MAT** for bitmap images. For domains with a concrete representation of the boundary, such as those with various spline or parametric representations of the boundary, **MA** and **MAT** are well-defined mathematically. For the domains with bitmap representation, there are various definitions of **MA** and **MAT** depending upon appli-


 Figure 14: The Letter A (a): Ω with its **MA**

cations, which are connected to various thinning methods [2],[3]. Nevertheless, there exist no unanimously agreed-upon definitions which are both theoretically natural and computable.

When $0 < 2\epsilon < \min \{ \rho \tan^2 \theta / 2, \rho / 2 \}$, we define a (ρ, θ, ϵ) -**MA** and a (ρ, θ, ϵ) -**MAT** of a domain Ω with bitmap representation, as the **MA** and **MAT** of any injective domain Ω' such that $\rho_{\Omega'} \geq \rho$, $\theta_{\Omega'} \geq \theta$, $\mathcal{H}(\partial\Omega', \partial\Omega) < \epsilon$ and $\mathcal{H}(\Omega', \Omega) < \epsilon$.


 Figure 15: The Letter A (b): Ω' with its **MA**

Then Theorem 3 guarantees that, for any injective domain Ω'' with $\rho_{\Omega''} \geq \rho$, $\theta_{\Omega''} \geq \theta$, $\mathcal{H}(\partial\Omega'', \partial\Omega) < \epsilon$ and $\mathcal{H}(\Omega'', \Omega) < \epsilon$, we have $\mathcal{H}(\mathbf{MA}(\Omega'), \mathbf{MA}(\Omega'')) < \eta$ and $\mathcal{H}(\mathbf{MAT}(\Omega'), \mathbf{MAT}(\Omega'')) < \sqrt{\eta^2 + (2\epsilon + \eta)^2}$, where $\eta = 2\rho\epsilon / (\rho^2 \sin^2 \theta/2 - 2\epsilon \cos^2 \theta/2)$. Furthermore, we have seen that $\mathbf{MA}(\Omega')$ and $\mathbf{MAT}(\Omega')$ have a “pruning effect” on $\mathbf{MA}(\Omega)$ and $\mathbf{MAT}(\Omega)$ respectively. These make the above definition a mathematically natural one.

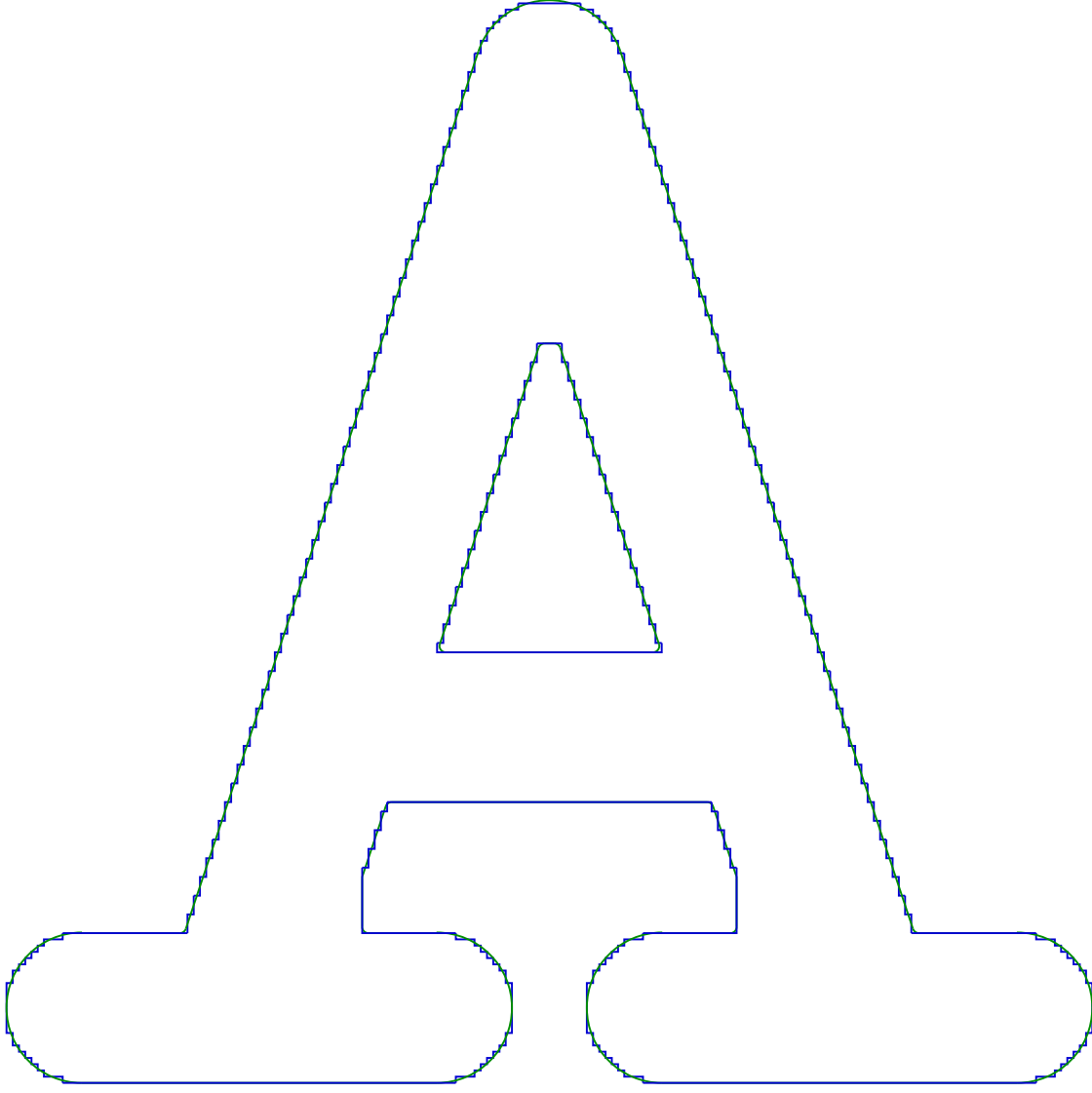


Figure 16: The Letter A (c) : Ω and Ω'

For the computation of a (ρ, θ, ϵ) -**MA** (and (ρ, θ, ϵ) -**MAT**), it suffices to compute the **MA** (and the **MAT**) of any one injective domain Ω' such that $\rho_{\Omega'} \geq \rho$, $\theta_{\Omega'} \geq \theta$, $\mathcal{H}(\partial\Omega'', \partial\Omega) < \epsilon$ and $\mathcal{H}(\Omega'', \Omega) < \epsilon$. Usually, the computations of the **MA** and **MAT** of Ω' are less complex than those of Ω . (Compare Figure 14 and Figure 15.) The computations can be facilitated by using recent algorithms for **MAT** of the free-form boundary domains such as [32].

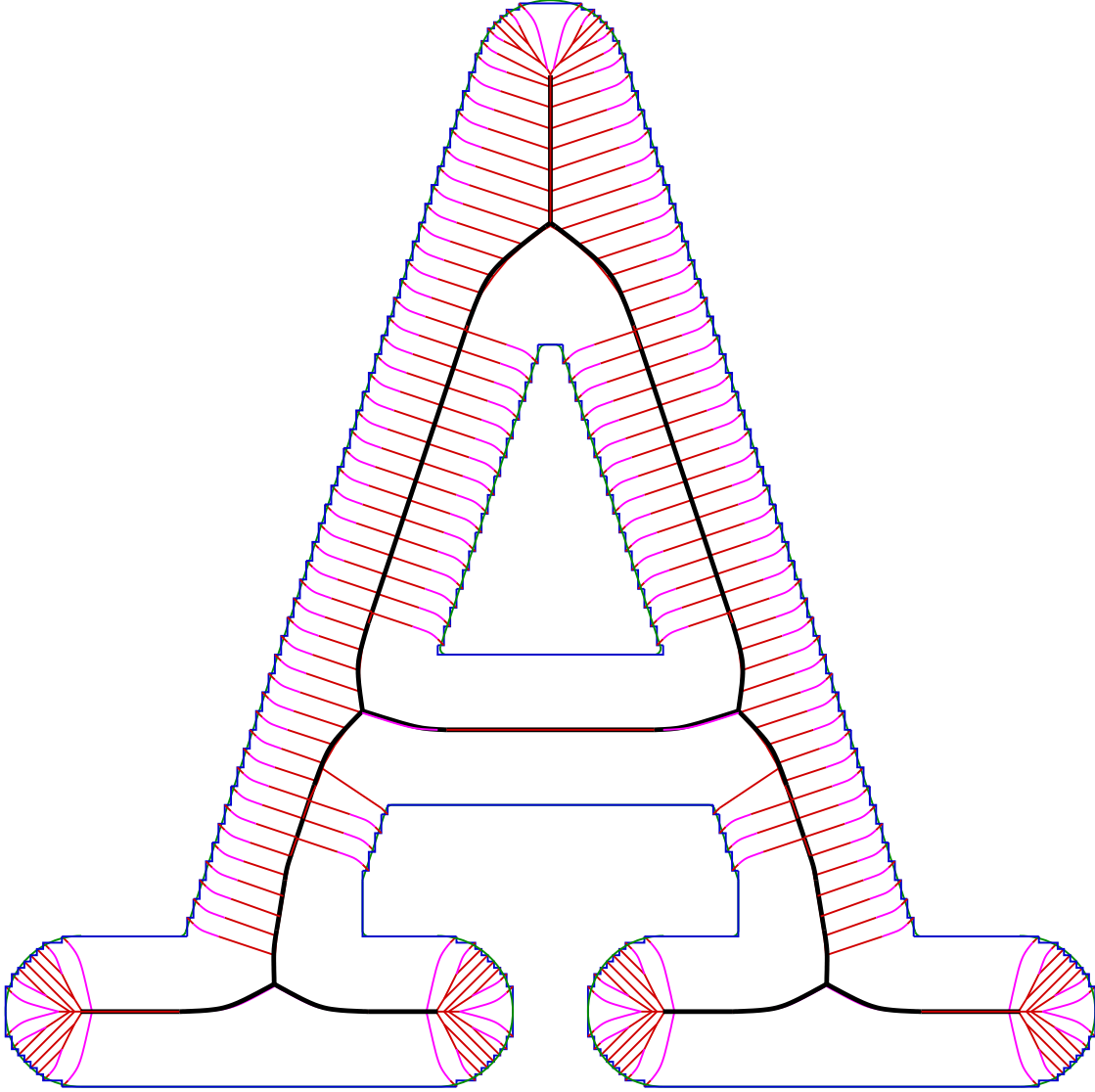


Figure 17: The Letter A (d): Ω and Ω' with their **MAs**

Thus, the above definition has the advantage of being both theoretically natural and amenable to computation.

6 CONCLUSION

We showed that the instability of medial axis transform can be resolved, by measuring the differences with respect to the relative Hausdorff distance. It

turned out that **MA** and **MAT** of injective domains are stable under relative Hausdorff distance. Furthermore, we derived a quantitative relation between the Hausdorff distance between the domains and the relative Hausdorff distance of one **MA** (*resp.*, **MAT**) with respect to the other **MA** (*resp.*, **MAT**). This was illustrated by simple but important examples.

By approximating a domain with an injective domain, this result makes it possible to extract the most essential part of **MA** and **MAT** of the domain within a prescribed error bound. In consequence, we can use this technique to devise a new pruning method with a precise upper bound for the errors, while there have been few significant error analyses in the previously known pruning methods. By applying our results on the stability of **MA** and **MAT** under relative Hausdorff distance, we also proposed a new definition of **MA** and **MAT** of the domains given by bitmap representation, which have the virtue of both naturalness and computability.

APPENDIX

PROOF OF THEOREM 1

Let $(p, r) \in \mathbf{MAT}(\Omega)$. Since Ω is injective, there exist at least two distinct points p_1 and p_2 in $\partial B_r(p) \cap \partial\Omega$. Define $0 \leq \theta \leq \pi/2$ by $\theta = (\angle p_1 p p_2)/2$. From the definition of θ_Ω , we may assume that $\theta \geq \theta_\Omega$. See Figure 18.

Note that $r - \epsilon > \epsilon$, since $\epsilon < \rho/2 \leq r/2$. Since $\mathcal{H}(\partial\Omega, \partial\Omega') < \epsilon$, we should have either $B_{r-\epsilon}(p) \subset \text{int}\Omega'$ or $B_{r-\epsilon}(p) \cap \Omega = \emptyset$. Suppose the latter. Then we would have $d(p, \Omega') > \epsilon$. But this contradicts the assumption that $\mathcal{H}(\Omega, \Omega') < \epsilon$.

29

Stability Analysis of MAT

which reduces to

$$\{r_0(1 - \cos \theta_\Omega) - 2\epsilon \cos \theta_\Omega\} \cdot \eta < 2\epsilon(r_0 + \epsilon). \quad (7)$$

Since $\rho_\Omega < r_0 + \epsilon$ and $\epsilon < \rho_\Omega \tan^2 \theta_\Omega / 2$, we have

$$(r_0 + \epsilon) \tan^2 \theta_\Omega / 2 > \epsilon,$$

which is equivalent to

$$2\epsilon \cos \theta_\Omega < r_0(1 - \cos \theta_\Omega).$$

This shows the left hand side of the equation (7) is positive. So from (7), we have

$$\eta < \frac{2\epsilon(r_0 + \epsilon)}{r_0(1 - \cos \theta_\Omega) - 2\epsilon \cos \theta_\Omega}. \quad (8)$$

It is easy to see that the right hand side of (8) is decreasing in r_0 . Thus we have

$$\begin{aligned} \eta &< \frac{2\epsilon\rho_\Omega}{(\rho_\Omega - \epsilon)(1 - \cos \theta_\Omega) - 2\epsilon \cos \theta_\Omega} \\ &= \frac{\epsilon\rho_\Omega}{\rho_\Omega \sin^2(\theta_\Omega/2) - \epsilon \cos^2(\theta_\Omega/2)} \\ &= \eta_\Omega(\epsilon), \end{aligned}$$

since $\rho_\Omega - \epsilon \leq r_0$. This proves $\mathcal{H}(\mathbf{MA}(\Omega)|\mathbf{MA}(\Omega')) < \eta_\Omega(\epsilon)$.

Suppose r' is the corresponding radius to p' , *i.e.*, $(p', r') \in \mathbf{MAT}(\Omega')$. Note that $r' = r_0 + \eta$. So $|r' - r| = |(r_0 - r) + \eta| \leq |r_0 - r| + \eta \leq \epsilon + \eta$. Thus we have

$$|(p', r') - (p, r)| < \sqrt{\eta^2 + (\epsilon + \eta)^2} < \sqrt{\eta_\Omega(\epsilon)^2 + \{\epsilon + \eta_\Omega(\epsilon)\}^2},$$

from which it follows that

$$\mathcal{H}(\mathbf{MAT}(\Omega)|\mathbf{MAT}(\Omega')) < \sqrt{\eta_\Omega(\epsilon)^2 + \{\epsilon + \eta_\Omega(\epsilon)\}^2},$$

and the proof is completed.

REFERENCES

- [1] H. Blum, “A tranformation for extracting new descriptors of shape,” *Proc. Symp. Models for the Perception of Speech and Visual Form* (W.W. Dunn, Ed.), MIT Press, Cambridge, MA, pp. 362–380, 1967.
- [2] L. Lam, S.-W. Lee and C.Y. Suen, “Thinning methodologies—a comprehensive survey,” *IEEE Trans. Pattern Analysis and Machine Intelligence*, vol. 14, no. 9, pp. 869–885, Sept. 1992.
- [3] C.Y. Suen and P.S.P Wang (Eds.), *Thinning Methodologies for Pattern Recognition*, World Scientific, 1994.
- [4] H.I. Choi, S.W. Choi and H.P. Moon, “Mathematical theory of medial axis transform,” *Pacific J. Math.*, vol. 181, no. 1, pp. 57–88, Nov. 1997.
- [5] A.R. Dill, M.D. Levine and P.B. Noble, “Multiple resolution skeletons,” *IEEE Trans. Pattern Analysis and Machine Intelligence*, vol. 9, no. 4, pp. 495–504, July 1987.
- [6] C.J. Hilditch, “An application of graph theory in pattern recognition,” *Machine Intell.* (B. Meltzer and D. Michie, Eds.), vol. 3, New York: Amer. Elsevier, pp. 325–347, 1968.
- [7] C.J. Hilditch, “Linear skeletons from square cupboards,” *Machine Intell.* (B. Meltzer and D. Michie, Eds.), vol. 4, New York: Amer. Elsevier, pp. 403–420, 1969.

- [8] N. Izzo and W. Coles, “Blood-cell scanner identifies rare cells,” *Electron.*, vol. 35, pp. 52–55, Apr. 1962.
- [9] T.V. Nguyen and J. Sklansky, “A fast skeleton-finder for coronary arteries,” *Proc. 8th Int. Conf. Patt. Recogn.*, (Paris, France), pp. 481–483, 1986.
- [10] K. Preston, “The CELLSCAN system—a leucocyte pattern analyzer,” *Proc. West. Joint Comput. Conf.*, (Los Angeles, CA), pp. 173–183, 1961.
- [11] K. Preston, M.J.B. Duff, S. Levialdi, P.E. Norgren and J.-I. Toriwaki, “Basics of cellular logic with some applications in medical image processing,” *Proceedings of the IEEE*, vol. 67, no. 5, pp. 826–857, 1979.
- [12] T.M. Alcorn and C.W. Hoggar, “Pre-processing of data for character recognition,” *Marconi Rev.*, vol. 32, pp. 61–81, 1969.
- [13] E.S. Deutsch, “Preprocessing for character recognition,” *Proc. IEEE NPL Conf. Patt. Recogn.*, (Teddington), pp. 179–190, 1968.
- [14] L. Lam and C.Y. Suen, “Structural classification and relaxation matching of totally unconstrained handwritten Zip-code numbers,” *Pattern Recognition*, vol. 21, no. 1, pp. 19–31, 1988.
- [15] H. Sherman, “A quasitopological method for the recognition of line patterns,” *Proc. Int. Conf. on Inform. Processing*, (Paris, France), pp. 232–238, 1959.

- [16] C.Y. Suen, M. Berthold and S. Mori, “Automatic recognition of handprinted characters,” *Proceedings of the IEEE*, vol. 68, no. 4, pp. 469–487, 1980.
- [17] C.C. Tappert, C.Y. Suen and T. Wakahara, “The state of the art in on-line handwriting recognition,” *IEEE Trans. Pattern Analysis and Machine Intelligence*, vol. 12, no. 8, pp. 787–808, Aug. 1990.
- [18] B. Moayer and K.S. Fu, “A syntactic approach of fingerprint pattern recognition,” *Pattern Recognition*, vol. 7, pp. 1–23, 1975.
- [19] Q.-Z. Ye and P.E. Danielsson, “Inspection of printed circuit boards by connectivity preserving shrinking,” *IEEE Trans. Pattern Analysis and Machine Intelligence*, vol. 10, no. 5, pp. 737–742, Sept. 1988.
- [20] D. Shaked and A.M. Bruckstein, “Pruning medial axis,” *Computer Vision and Image Understanding*, vol. 69, no. 2, pp. 156–169, Feb. 1998.
- [21] J. August, A. Tannenbaum and S.W. Zucker, “On the evolution of the skeleton,” *Proc. 7th Int’l Conf. Computer Vision*, (Kerkyra, Greece), Sept. 1999 (to appear).
- [22] M.P. Deseilligny, G. Stamon and C.Y. Suen, “Veinerization: A new shape descriptor for flexible skeletonization,” *IEEE Trans. Pattern Analysis and Machine Intelligence*, vol. 20, no. 5, pp. 505–521, May 1998.
- [23] M. Gage and R. Hamilton, “The shrinking of convex plane curves by the heat equation,” *J. Diff. Geometry*, vol. 23, pp. 69–96, 1986.

- [24] C. Gerhardt, “Flow of nonconvex hypersurfaces into spheres,” *J. Diff. Geometry*, vol. 32, pp. 299–314, 1990.
- [25] M. Grayson, “The heat equation shrinks embedded plane curves to round points,” *J. Diff. Geometry*, vol. 26, pp. 285–314, 1987.
- [26] F. Mokhtarian and A.K. Mackworth, “A theory of multiscale, curvature-based shape representation for planar curves,” *IEEE Trans. Pattern Analysis and Machine Intelligence*, vol. 14, no. 8, pp. 789–805, Aug. 1992.
- [27] S. Osher and J.A. Sethian, “Fronts propagating with curvature-dependent speed: Algorithm based on Hamilton-Jacobi formulation,” *Journal of Computational Physics*, vol. 79, pp. 12–49, 1988.
- [28] J.A. Sethian, “Numerical algorithms for propagating interfaces: Hamilton-Jacobi equations and conservation laws,” *J. Diff. Geometry*, vol. 31, pp. 131–161, 1990.
- [29] H.I. Choi, D.S. Lee and J.-H. Yoon, “Cut locus of a separating fractal set in a Riemannian manifold,” *Tohoku Math. J. (2)*, vol. 50, no. 4, pp. 455–467, 1998.
- [30] M. Barnsley, *Fractals Everywhere*, Academic Press, 1988.
- [31] F.P. Preparata and M.I. Shamos, *Computational Geometry*, Springer-Verlag, 1985.

- [32] H.I. Choi, S.W. Choi, H.P. Moon and N.-S. Wee, “New algorithm for medial axis transform of plane domain,” *Graphical Models and Image Processing*, vol. 59, no. 6, pp. 463–483, Nov. 1997.